Electronic Supplementary Material (ESI) for Journal of Materials Chemistry A.

# Electronic Supplementary Information

## Influence of Fluorination on $CO_2$ Adsorption in Materials Derived from Fluorinated Covalent Triazine Framework Precursors

Zhenzhen Yang,[a, b] Song Wang,[c] Zihao Zhang,[a] Wei Guo,[a] Kecheng Jie,[a] Mohamed I. Hashim,[d] Ognjen Š. Miljanic,[d] De-en Jiang,[c] Ilja Popovs,[b,] * Sheng Dai[a, b,] *

# Table of Contents

# 1 Experimental Procedures

## 1.1 Materials

All reagents and solvents were purchased from commercial sources and were used without further purification, unless indicated otherwise.

## 1.2 Characterization

FTIR spectra of the samples were collected on a TENSOR 27 FTIR at a resolution of 2 $cm^{-1}$. solid-state $^{13}C$ NMR was performed using a Solid State Varian INOVA 400 MHz. Powder X-ray diffraction (XRD) data were recorded with a PANalytical Empyrean diffractometer, operated at 45 kV and 40 mA (scanning step: 0.02° per step). The diffraction patterns were recorded in the range of 5-60° 2θ. X-ray photoelectron spectroscopy (XPS) measurements: XPS experiments were performed with a PHI 3056 spectrometer equipped with an Al anode source operated at 15 KV and an applied power of 350 W and a pass energy of 93.5 eV. Samples were mounted on In foil since the C1s binding energy was used to calibrate the binding energy shifts of the sample (C1s = 284.8 eV). The nitrogen adsorption and desorption isotherms were measured at 77 K under a Gemini 2360 surface area analyzer. The samples were outgassed at 150 $^{o}$C for 16 h before the measurements. Surface areas were calculated from the adsorption data using Brunauer-Emmett-Teller (BET) methods. The pore-size-distribution curves were obtained from the adsorption branches using non-local density functional theory (NLDFT) method. The $CO_2$ adsorption and desorption isotherms were measured at 273 K by Autosorb-1-C Quantachrome analyzer. Elemental analyses were performed by Atlantic Microlab Inc., Norcross, GA.

## 1.3 Heat of $CO_2$ Adsorption Calculation

The isosteric heat of adsorption values were calculated using the Clausius-Clapeyron equation:

$$\ln\left(\frac{P_1}{P_2}\right) = \Delta H_{ads} \times \frac{T_2 - T_1}{R \times T_1 \times T_2}$$

where $P_i$ is pressure for isotherm *i*, $T_i$ is temperature for isotherm *i*, *R* is 8.315 J $K^{-1}$ $mol^{-1}$; which was used to calculate isosteric heat of adsorption ($\Delta H_{ads}$) of a gas as a function of the quantity of gas adsorbed.

Pressure as a function of the amount of CO2 adsorbed was determined by the Toth model for the isotherms.

$$Q = \frac{Q_m \times B^{(1/t)} P_1}{(1 + B \times P)^{1/t}}$$

where *Q* = moles adsorbed, $Q_m$ = moles adsorbed at saturation, *P* = pressure; *B* and *t* =constants; which can be used to calculate the pressure *P*.

## 1.4 Synthesis of Monomers

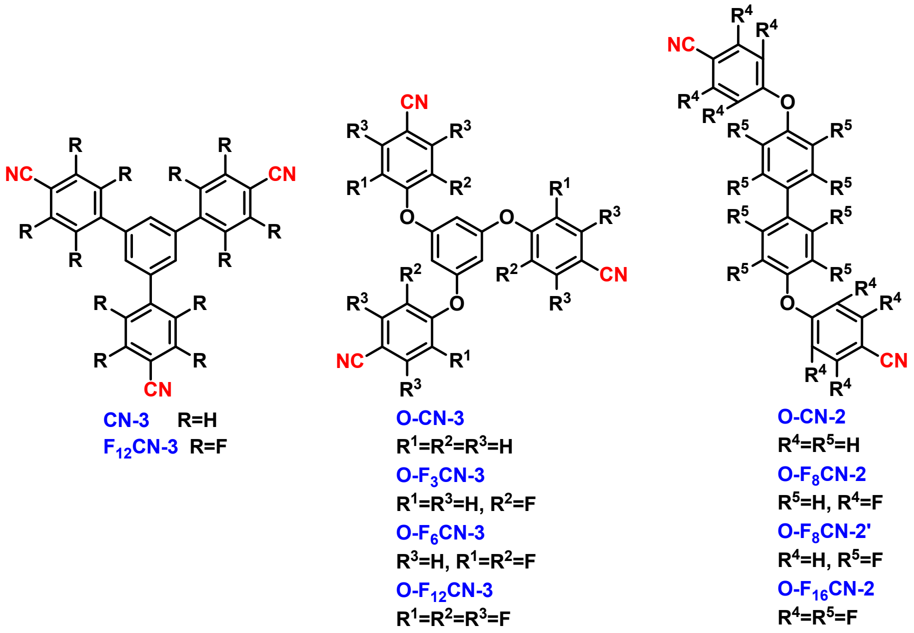

**Scheme S1** Structures of fluorinated nitriles used in this study.

Commercially available starting materials and solvents were purchased from vendors and were used without further purification unless noted otherwise. The $^1$H and $^{19}$F NMR spectra were recorded on Bruker 400 spectrometer using the residual solvent peaks, tetramethylsilane or α,α,α-trifluorotoluene ($\delta CF_3$ = -62.61 p.p.m.) as the internal standard respectively. $^{13}$C Spectra were not included since they are not informative, due to extensive coupling between $^{13}$C and $^{19}$F nuclei, low intensity and number of missing peaks. 1,3,5-tris((trimethylsilyl)oxy)benzene,[1] 5'-(4-cyanophenyl)-[1,1':3',1''-terphenyl]-4,4''-dicarbonitrile (**CN-3**),[2] 5'-(4-cyano-2,3,5,6-tetrafluorophenyl)-2,2'',3,3'',5,5'',6,6''-octafluoro-[1,1':3',1''-terphenyl]-4,4''-dicarbonitrile (**F$_{12}$CN-3**),[3, 4] and 4,4',4''-(Benzene-1,3,5-triyltris(oxy))tribenzonitrile (**O-CN-3**)[4, 5] were prepared according to published methods.

**Synthesis of 4,4',4''-(benzene-1,3,5-triyltris(oxy))tris(3-fluorobenzonitrile) (O-F$_3$CN-3)**

The reaction flask (250 mL) containing magnetic stirring bar was charged with 1,3,5-tris((trimethylsilyl)oxy)benzene (10.28 g, 30 mmol), followed by the addition of 3,4 -difluorobenzonitrile (13.90 g, 100 mmol). The reaction flask was purged with Argon, and anhydrous DMF (100 mL) was added. Anhydrous cesium fluoride (1.52 g, 10 mmol) was carefully added in one portion, the reaction flask was capped with a septum connected to a bubbler and stirred at 120 °C for 24 hours. The reaction mixture was poured in water under vigorous stirring and the resulting precipitate was filtered off and air dried. The title product was obtained after the re-crystallization from ethanol. The product was obtained after filtration as a white powder (9.2 g, 63 %).

$^1$H NMR (CDCl$_3$, 400 MHz) δ 6.48 (s, 3H), 7.15 (t, $^3J$ = 8 Hz, 3H), 7.45~7.51 (m, 6H); $^{19}$F NMR (CDCl$_3$, 376 Hz) δ -126.76 (t, 3J = 9.02 Hz, 3 F).

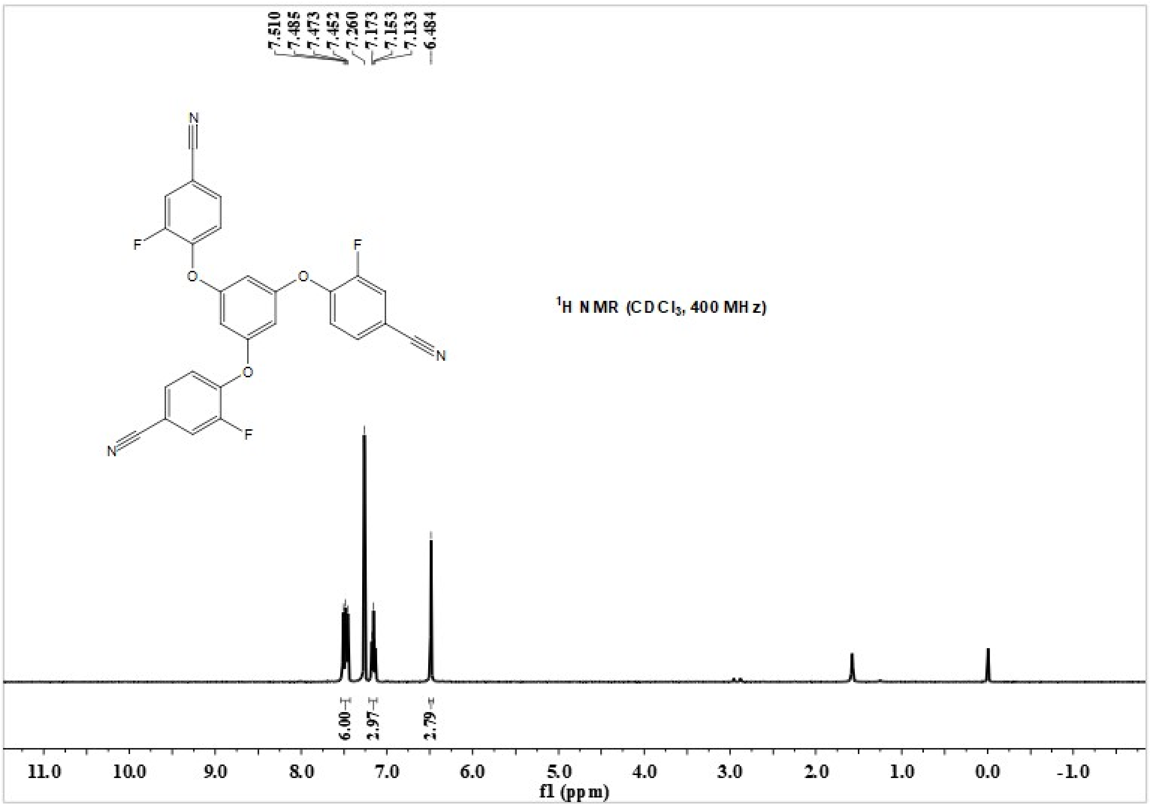

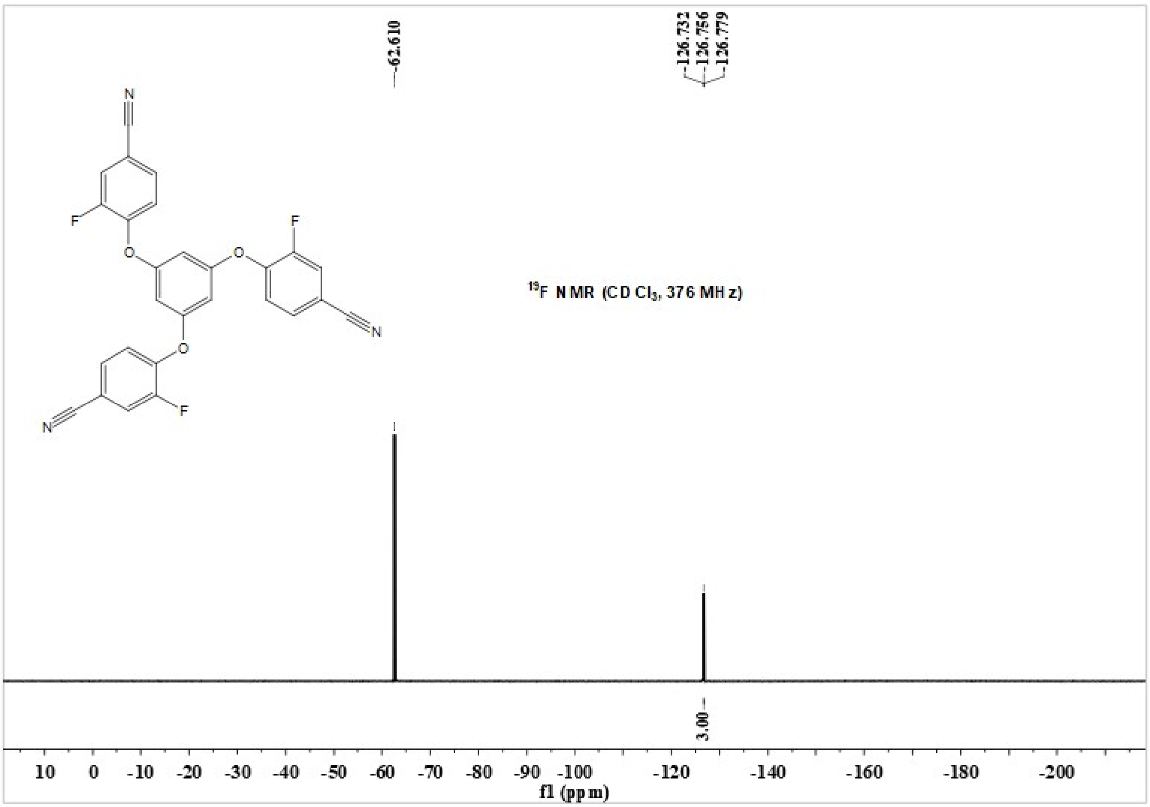

**Synthesis of 4,4',4''-(benzene-1,3,5-triyltris(oxy))tris(3,5-difluorobenzonitrile) (O-$F_6$CN-3)**

The reaction flask (250 mL) containing magnetic stirring bar was charged with 1,3,5-tris((trimethylsilyl)oxy)benzene (10.28 g, 30 mmol), followed by the addition of 3,4,5-trifluorobenzonitrile (15.71 g, 100 mmol). The reaction flask was purged with Argon, and anhydrous DMF (100 mL) was added. Anhydrous cesium fluoride (1.52 g, 10 mmol) was carefully added in one portion, the reaction flask was capped with a septum connected to a bubbler and stirred at room temperature for 24 hours. The reaction mixture was poured in water under vigorous stirring and the resulting precipitate was filtered off and air dried. The title product was obtained after the re-crystallization from methanol. The product was obtained after filtration as a white powder (15.0 g, 93 %).

$^{1}$H NMR ($CDCl_3$, 400 MHz) δ 6.30 (s, 3H), 7.34~7.40 (m, 6H); $^{19}$F NMR ($CDCl_3$, 376 Hz) δ -121.14 (d, $^{3}J$ = 6.8 Hz, 6F).

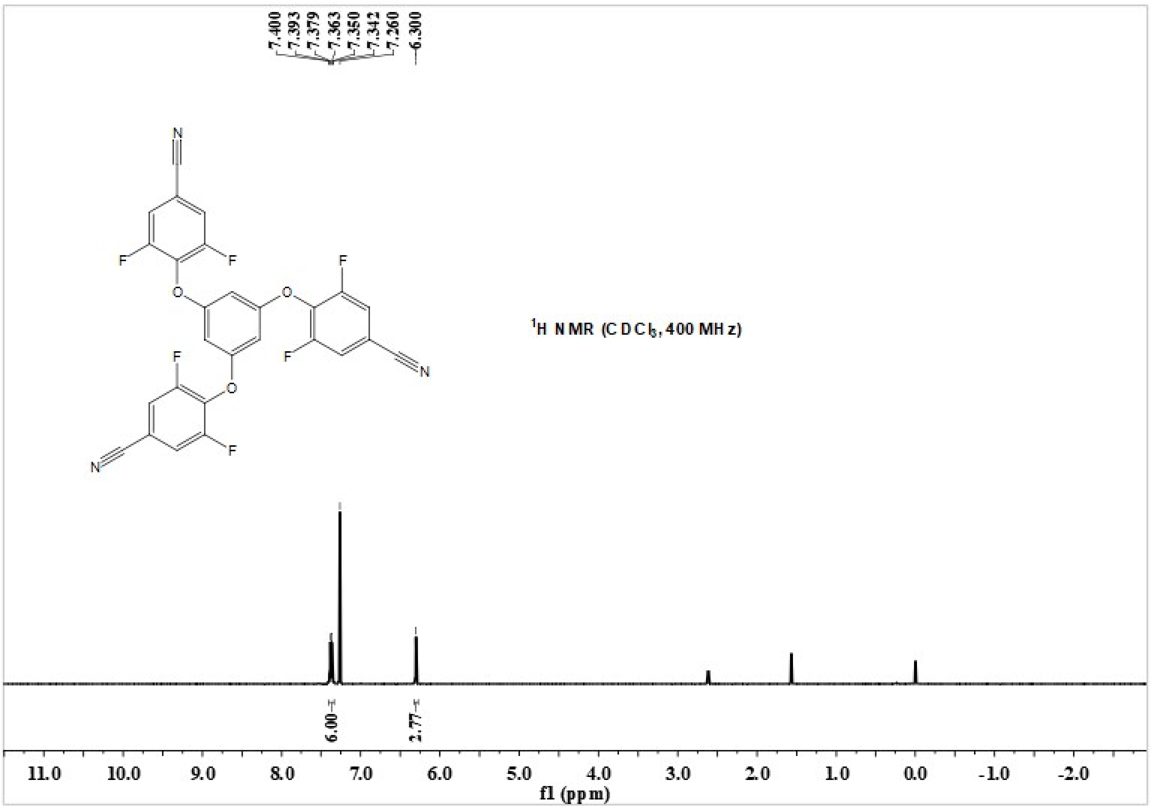

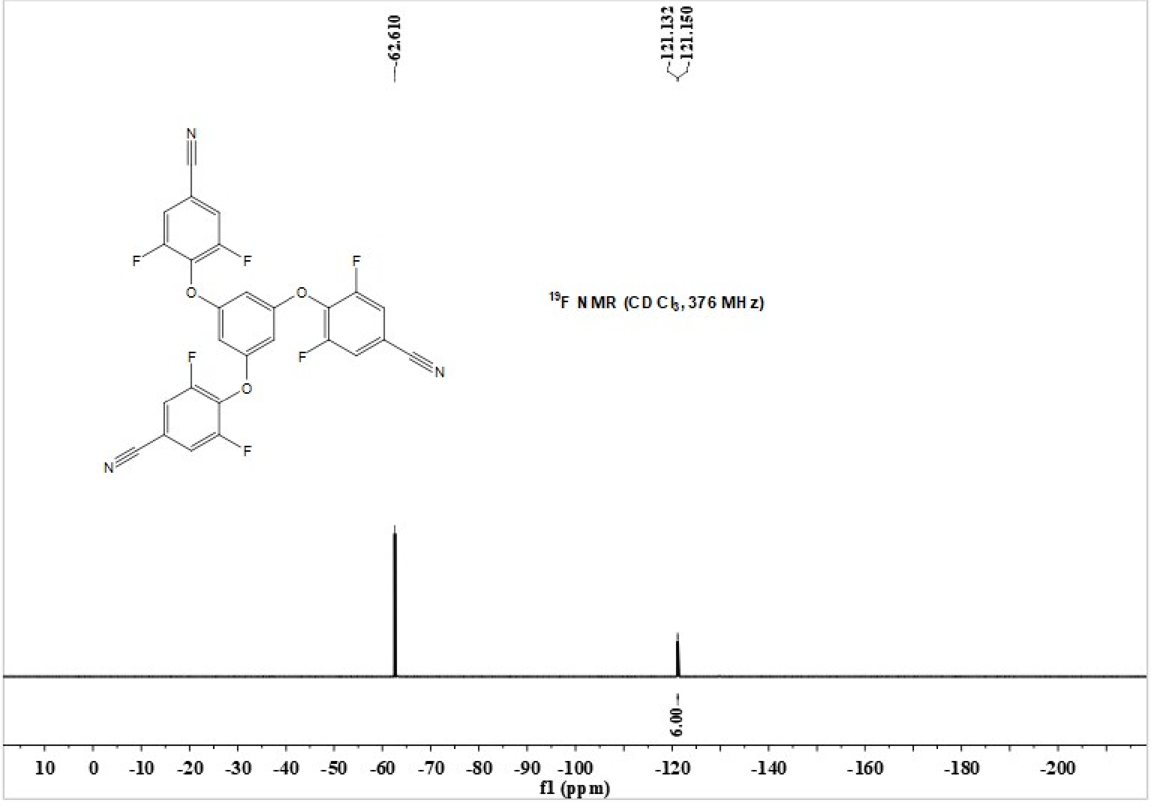

**Synthesis of 4,4',4''-(benzene-1,3,5-triyltris(oxy))tris(2,3,5,6-tetrafluorobenzonitrile) (O-$F_{12}$CN-3)**

The reaction flask (250 mL) containing magnetic stirring bar was charged with 1,3,5-tris((trimethylsilyl)oxy)benzene (10.28 g, 30 mmol), followed by the addition of pentafluorobenzonitrile (19.3 g, 100 mmol). The reaction flask was purged with Argon, and anhydrous DMF (100 mL) was added. Anhydrous cesium fluoride (1.52 g, 10 mmol) was carefully added in one portion, the reaction flask was capped with a septum connected to a bubbler and stirred at room temperature for 24 hours. The reaction mixture was poured in water under vigorous stirring and the resulting precipitate was filtered off and air dried. The title product was obtained after the re-crystallization from methanol. The product was obtained after filtration as a white powder (12.58 g, 67 %).

$^1$H NMR ($CDCl_3$, 400 MHz) δ 6.49 (s, 3H); $^{19}$F NMR ($CDCl_3$, 376 Hz) δ -149.65~-149.55 (m, 6F), -130.49~-130.38 (m, 6F).

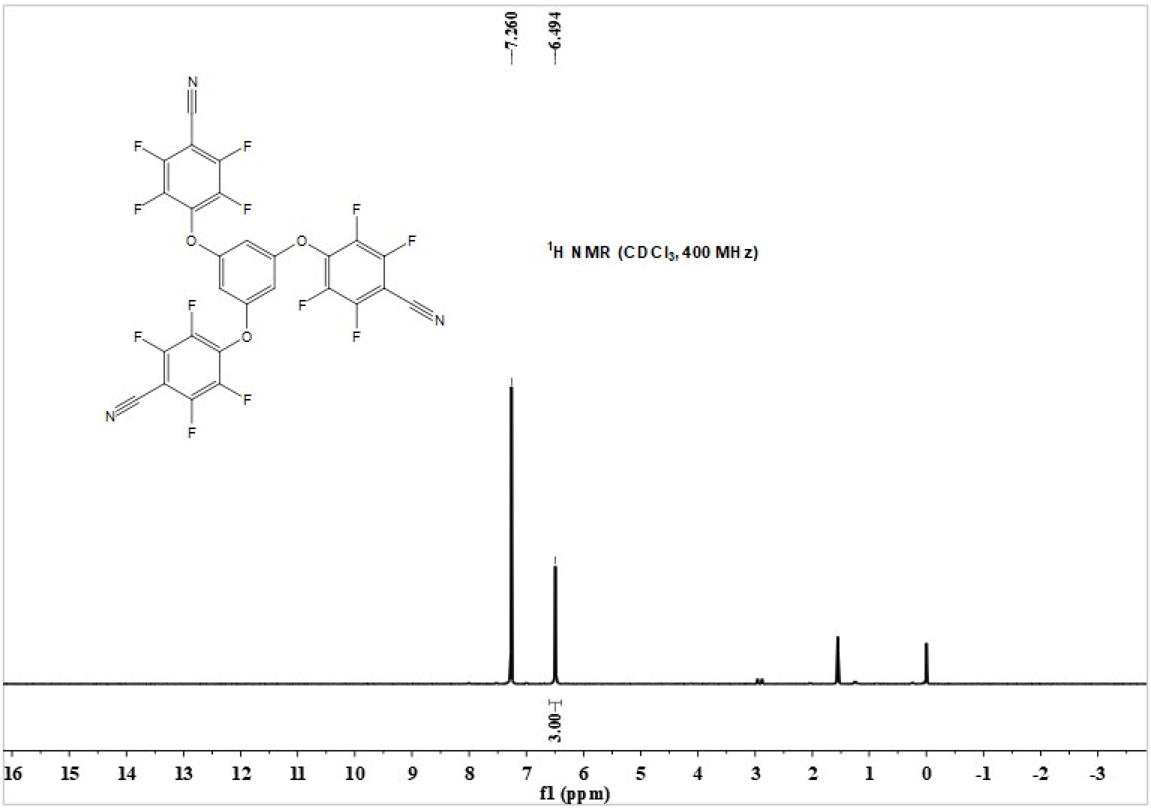

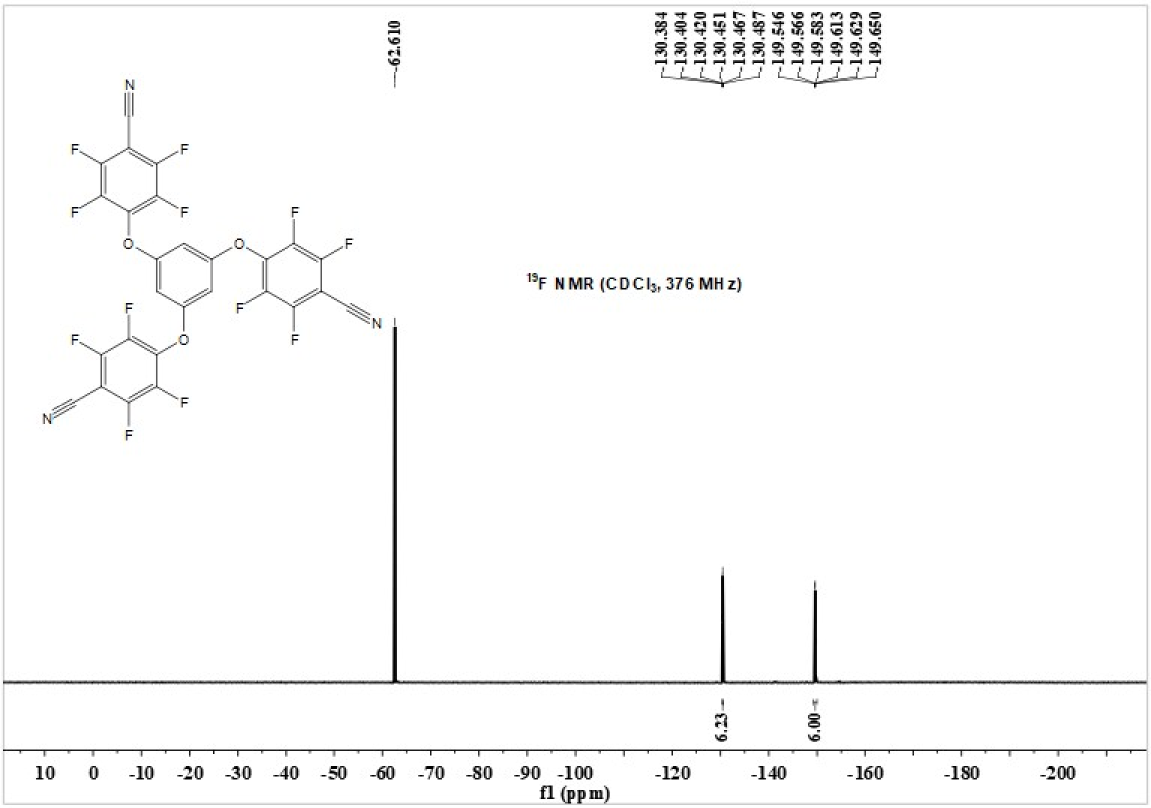

**Synthesis of 4,4'-([1,1'-biphenyl]-4,4'-diylbis(oxy))dibenzonitrile (O-CN-2)**

The reaction flask (300 mL) containing magnetic stirring bar was charged with [1,1'-biphenyl]-4,4'-diol (5.59 g, 30 mmol), followed by the addition of 4-fluorobenzonitrile (9.69 g, 80 mmol). The reaction flask was purged with Argon, and anhydrous DMSO (200 mL) was added. Anhydrous potassium carbonate (10.37 g, 75 mmol) was added in one portion, the reaction flask was capped with a septum and stirred at 150 °C for 8 hours. Additional amount of 4-fluorobenzonitrile (9.69 g, 80 mmol) was introduced and the reaction mixture was stirred at 150 °C for another 8 hours. The reaction mixture was poured in water under vigorous stirring and the resulting precipitate was filtered off and air dried. The title product was obtained after the re-crystallization from DMSO. The product was obtained after filtration as a white powder (7.35 g, 63 %).

$^{1}$H NMR (CDCl$_3$, 400 MHz) δ 7.07 (d, $^{3}J$ = 8.8 Hz, 4H), 7.15 (d, $^{3}J$ = 8.8 Hz, 4H), 7.62 (t, $^{3}J$ = 8.8 Hz, 8H);

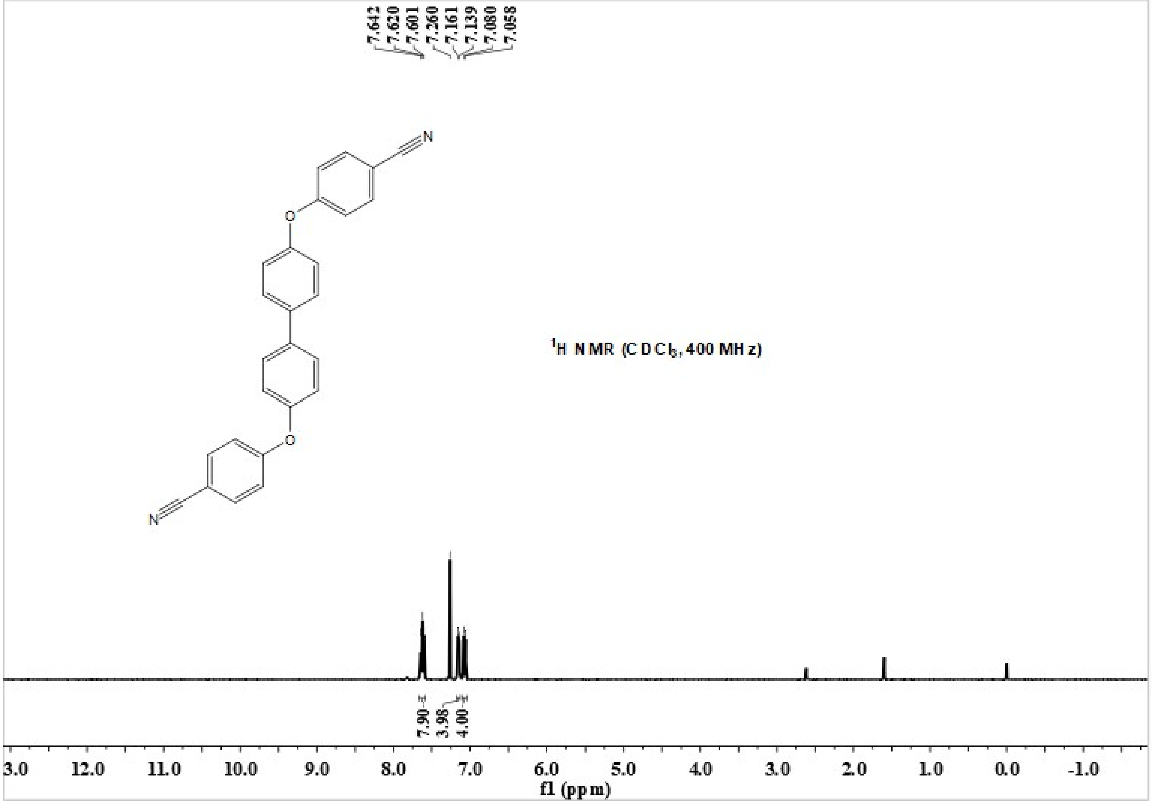

### Synthesis of 4,4'-((perfluoro-[1,1'-biphenyl]-4,4'-diyl)bis(oxy))dibenzonitrile (O-$F_8$CN-2)

The reaction flask (300 mL) containing magnetic stirring bar was charged with [1,1'-biphenyl]-4,4'-diol (5.59 g, 30 mmol), followed by the addition of pentafluorobenzonitrile (15.44 g, 80 mmol). The reaction flask was purged with Argon, and anhydrous DMSO (200 mL) was added. Anhydrous potassium carbonate (10.37 g, 75 mmol) was added in one portion, the reaction flask was capped with a septum and stirred at room temperature for 24 hours. The reaction mixture was poured in water under vigorous stirring and the resulting precipitate was filtered off and air dried. The title product was obtained after the re-crystallization from isopropanol. The product was obtained after filtration as a white powder (10.0 g, 63 %).

$^1$H NMR (CDCl$_3$, 400 MHz) δ 7.08 (d, $^3J$ = 8.8 Hz, 4H), 7.54 (d, $^3J$ = 8.8 Hz, 4H); $^{19}$F NMR (CDCl$_3$, 376 Hz) δ -150.26~-150.16 (m, 4F), -131.74~-131.63 (m, 4F).

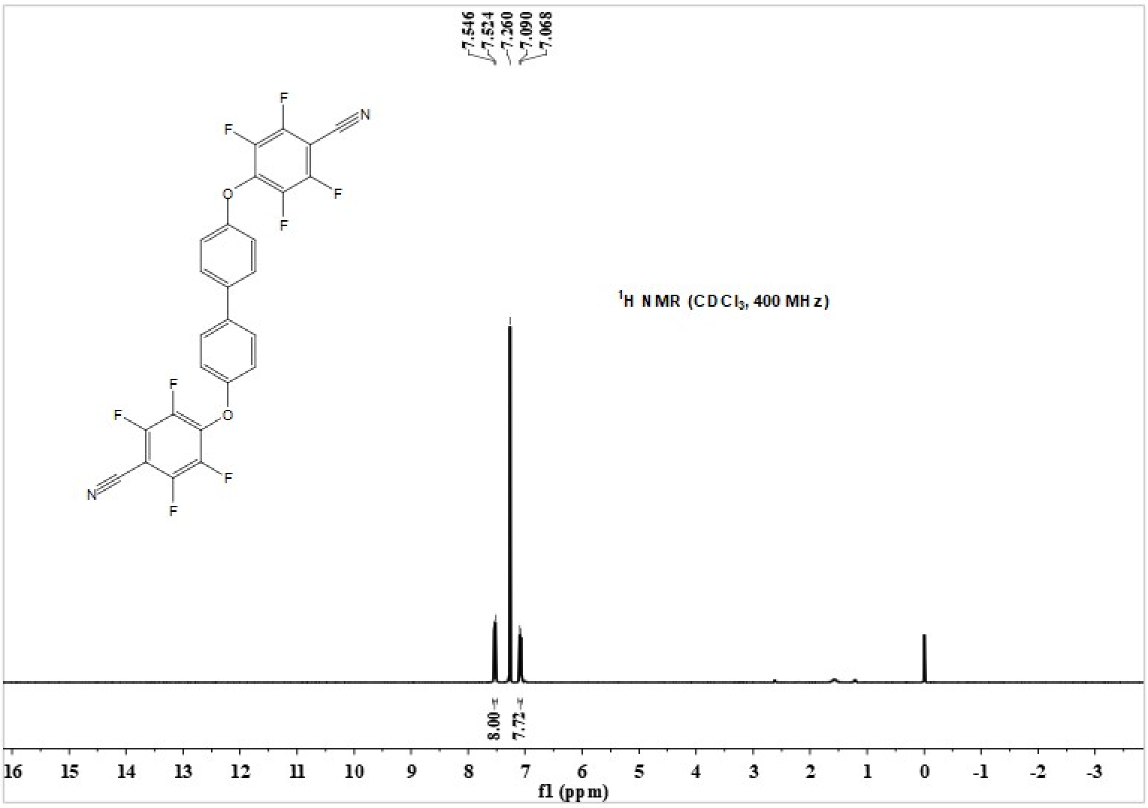

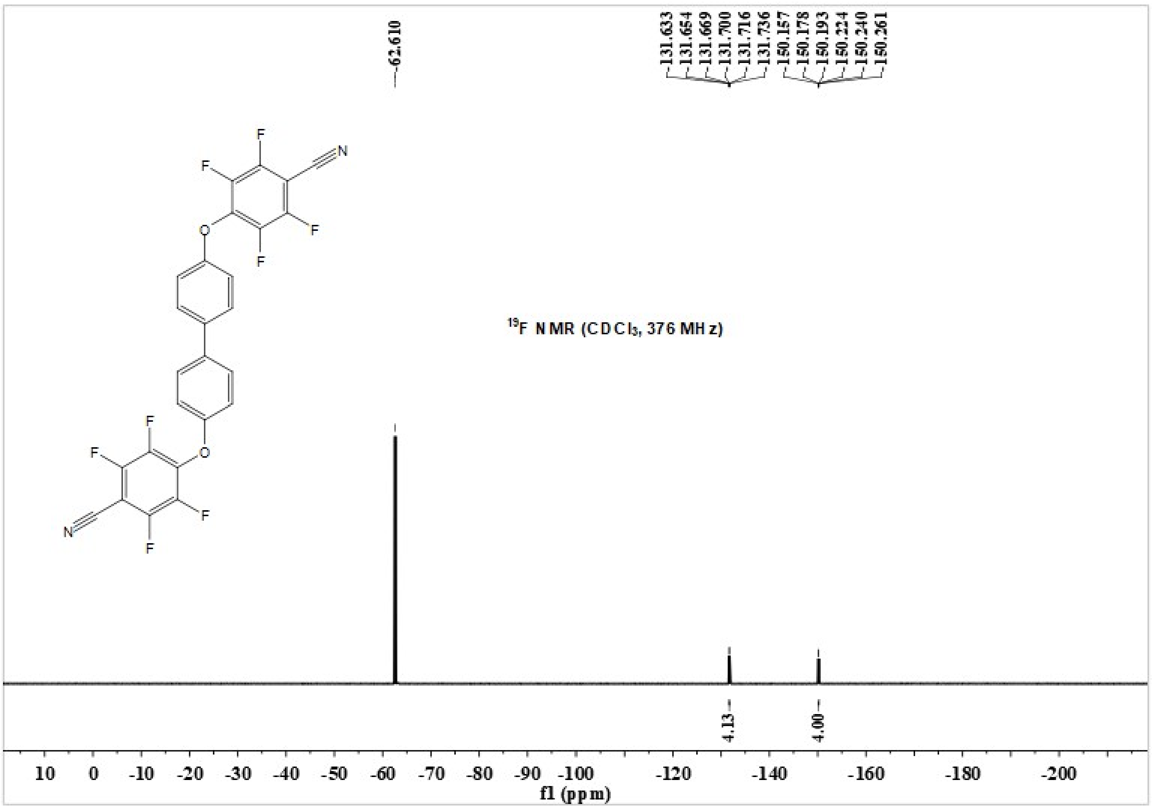

**Synthesis of 4,4'-([1,1'-biphenyl]-4,4'-diylbis(oxy))bis(2,3,5,6-tetrafluorobenzonitrile) (O-$F_8$CN-2')**

The reaction flask (250 mL) containing magnetic stirring bar was charged with perfluoro-1,1'-biphenyl (6.68 g, 20 mmol), followed by the addition of 4-hydroxybenzonitrile (5.35 g, 45 mmol). The reaction flask was purged with Argon, and anhydrous DMSO (70 mL) was added. Anhydrous potassium carbonate (8.30 g, 60 mmol) was added in one portion, the reaction flask was capped with a septum and stirred at 100

°C for 2 hours. The reaction mixture was poured in water under vigorous stirring and the resulting precipitate was filtered off and air dried. The title product was obtained after the re-crystallization from isopropanol. The product was obtained after filtration as a white powder (9.7 g, 91 %).

$^1$H NMR (CDCl$_3$, 400 MHz) δ 7.14 (d, $^3J$ = 8.8 Hz, 4H), 7.71 (d, $^3J$ = 8.8 Hz, 4H); $^{19}$F NMR (CDCl$_3$, 376 Hz) δ -151.90~-151.84 (m, 4F), -136.64~-136.57 (m, 4F).

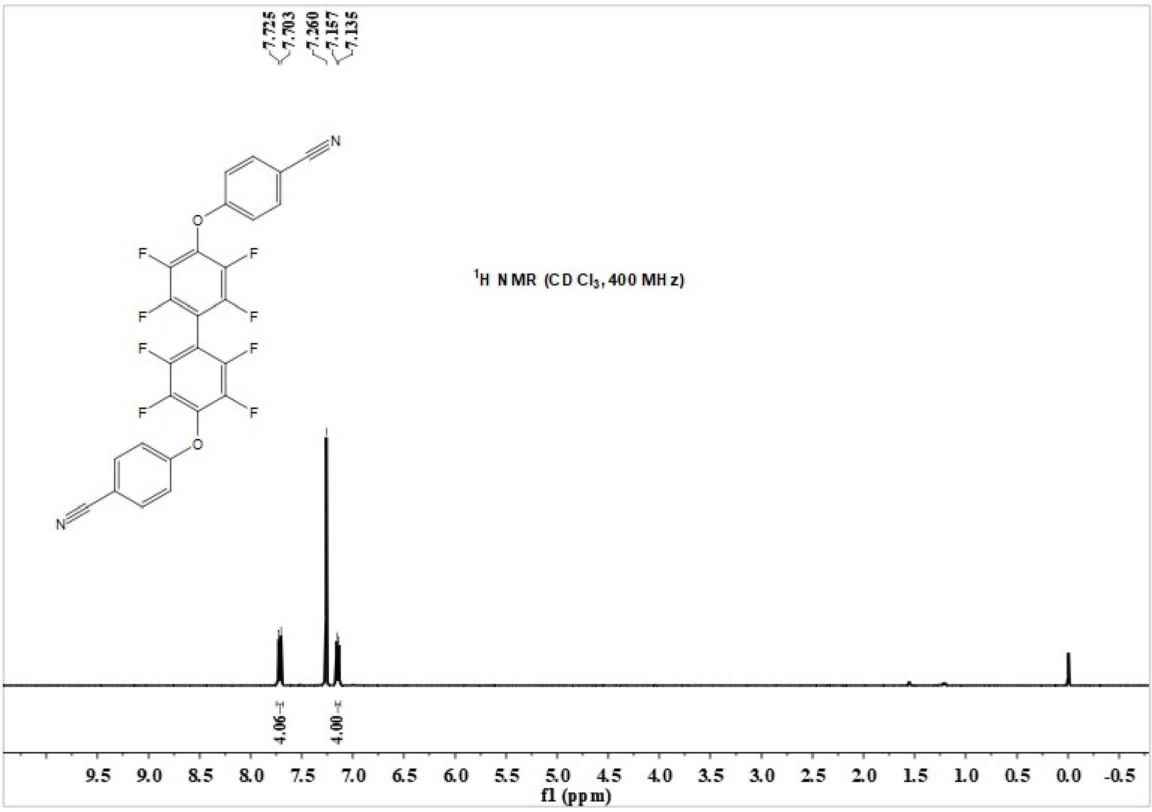

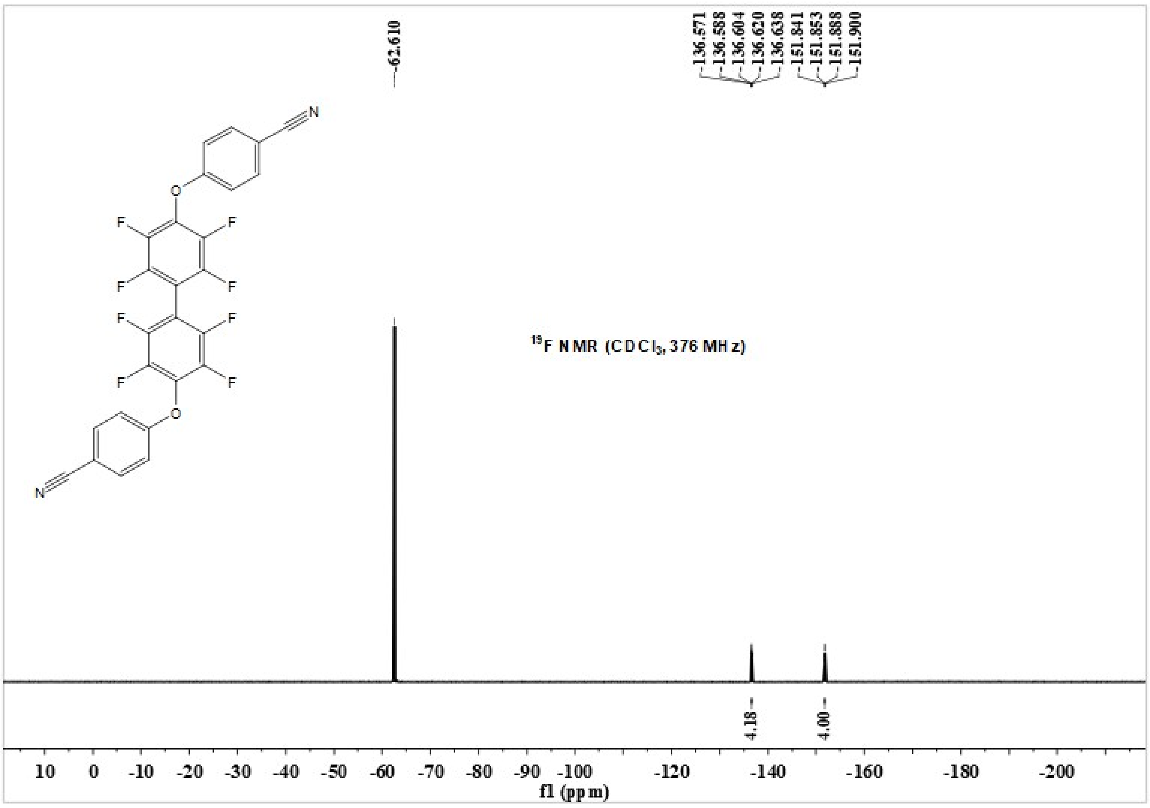

**Synthesis of 4,4'-((2,2',3,3',5,5',6-heptafluoro-[1,1'-biphenyl]-4,4'-diyl)bis(oxy))bis(2,3,5,6-tetrafluorobenzonitrile) (O-F$_{16}$CN-2)**

The reaction flask (250 mL) containing magnetic stirring bar was charged with 2,2',3,3',5,5',6,6'-octafluoro-[1,1'-biphenyl]-4,4'-diol (6.60 g, 20 mmol), followed by the addition of pentafluorobenzonitrile (11.68 g, 60 mmol). The reaction flask was purged with Argon, and anhydrous DMSO (100 mL) was added. Anhydrous potassium carbonate (6.91 g, 50 mmol) was added in one portion, the reaction flask was capped with a septum and stirred at 120 °C for 2 hours. The reaction mixture was poured in water under vigorous stirring and the resulting precipitate was filtered off and air dried. The title product was obtained after the re-crystallization from ethanol. The product was obtained after filtration as a white powder (4.9 g, 36 %).

$^{19}$F NMR (CDCl$_3$, 376 Hz) δ -154.35 (d, $^{3}J$ = 15.0 Hz, 4F), -152.64~-152.54 (m, 4F), -136.13~-136.06 (m, 4F), -130.74~-130.64 (m, 4F).

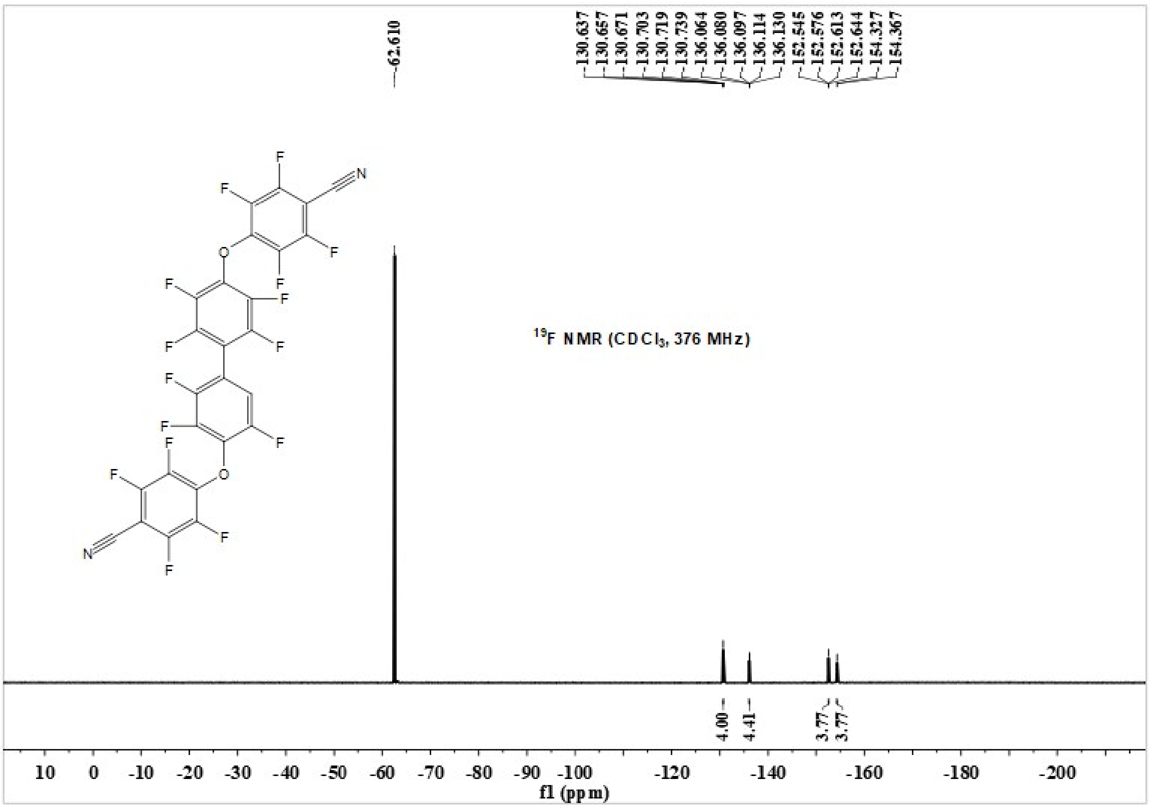

## 1.5 Preparation of CTF Materials

**Notes: Volatile products, maybe CF$_4$, C$_2$F$_4$ and F$_2$, are produced during the reaction. After cooling down to room temperature, the quartz tube must be immersed in liquid nitrogen for ~10 min, and then opened carefully in the hood.**

**CTF** materials were synthesized by ZnCl$_2$-catalyzed ionothermal method.[6] Typically, the synthesis of **F$_{12}$CTF-3** was shown as the following: A mixture of 5'-(4-cyano-2,3,5,6-tetrafluorophenyl)-2,2'',3,3'',5,5'',6,6''-octafluoro-[1,1':3',1''-terphenyl]-4,4''-dicarbonitrile (**F$_{12}$CN-3**) (0.6 mmol, 304 mg) and ZnCl$_2$ (6.0 mmol, 819 mg, 10:1) was vacuum-sealed in a quartz tube, and then heated at 450 °C for 20 h in a muffle furnace (5 °C/min). After that, the temperature was increased to 600 °C and maintained for another 20 h. The obtained black powder was subsequently ground and washed thoroughly with dilute HCl, water, THF and acetone. The material was then dried in an oven at 120 °C for 24 h.

**CTF-3**, **O-CTF-3**, **O-F$_3$CTF-3**, **O-F$_6$CTF-3**, **O-F$_{12}$CTF-3**, **O-CTF-2**, **O-F$_8$CTF-2**, **O-F$_8$CTF-2'**, **O-F$_{16}$CTF-2** were prepared using the corresponding monomers, the molar ratio of nitrile monomer: ZnCl$_2$ is 1:10.

**F$_{12}$CTF-3-350**, **F$_{12}$CTF-3-450**, and **F$_{12}$CTF-3-600** was prepared at the target temperature (400 °C, 450 °C and 600 °C) for 40 h, respectively. **F$_{12}$CTF-3-450/800** was prepared by heating at 450 $^{o}$C for 20 h and then 800 $^{o}$C for 20 h.

## 2 Results and Discussion

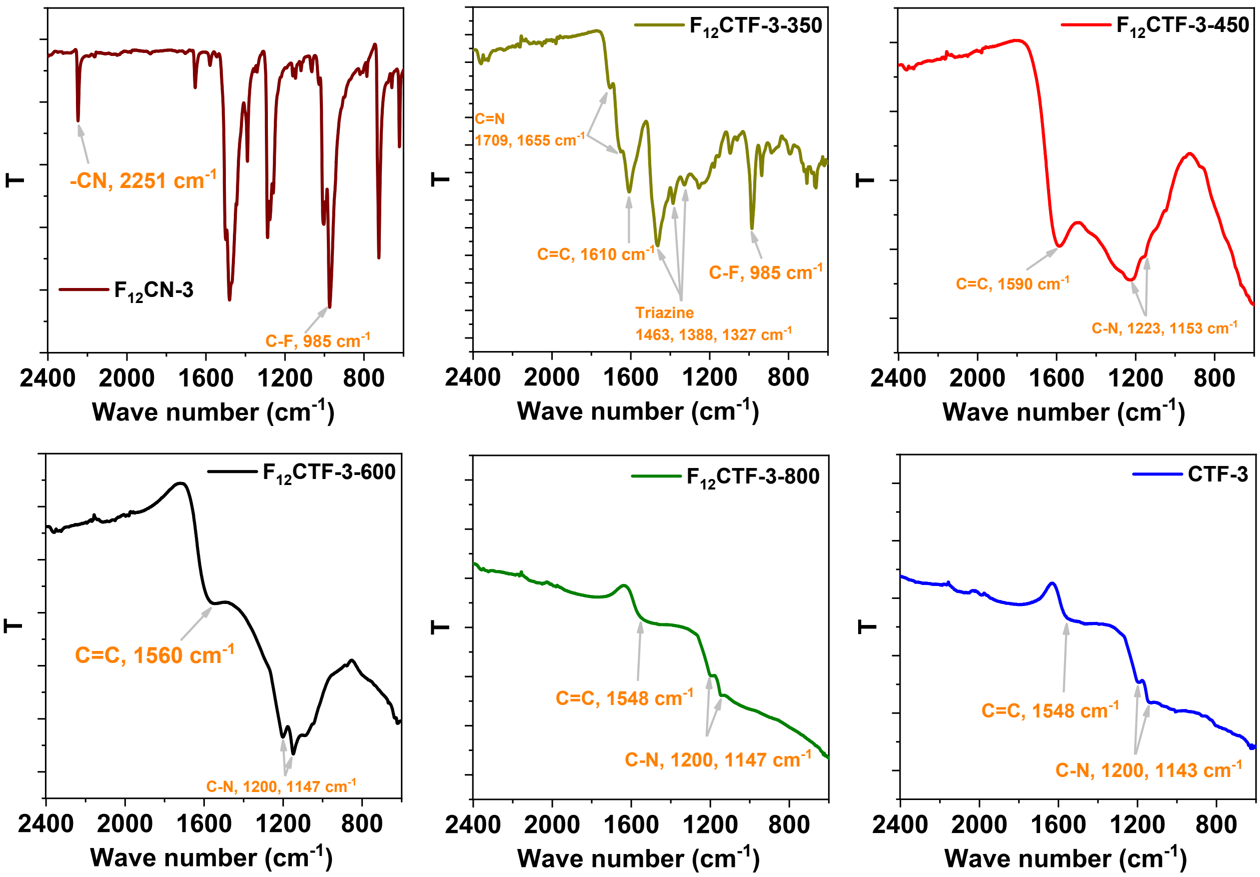

**Figure S1** Fourier-transform infrared (FT-IR) spectroscopy of **F$_{12}$CTF-3** and **CTF-3**.

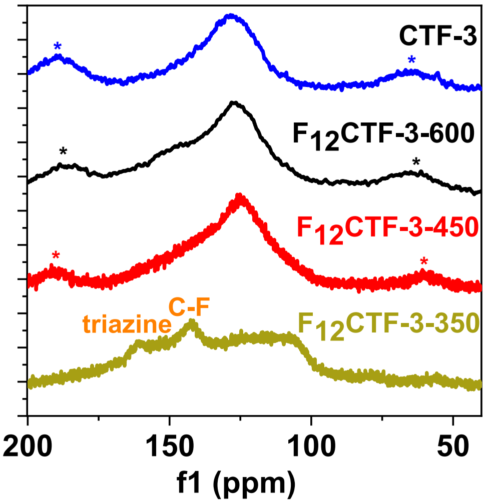

**Figure S2** Solid state $^{13}$C cross-polarization magic-angle-spinning (CP/MAS) NMR spectra of **$F_{12}$CTF-3** and **CTF-3**.

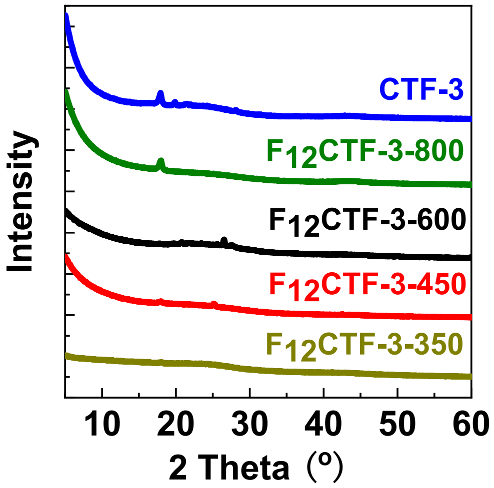

**Figure S3** X-ray power diffraction (XRD) patterns for **$F_{12}$CTF-3** and **CTF-3**.

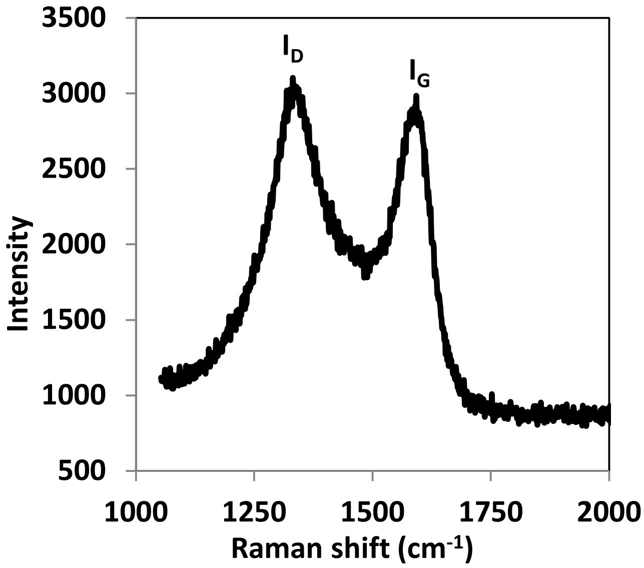

**Figure S4** Raman spectra of **$F_{12}$CTF-3**.

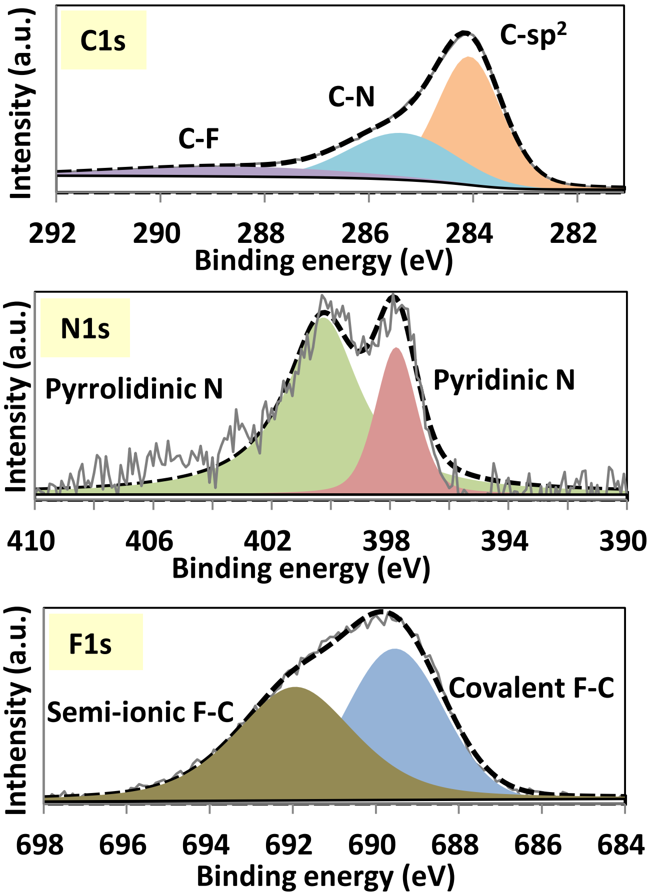

**Figure S5** X-rayphotoelectron spectroscopy (XPS) spectra (C1s, N1s, F1s) of **F$_{12}$CTF-3**.

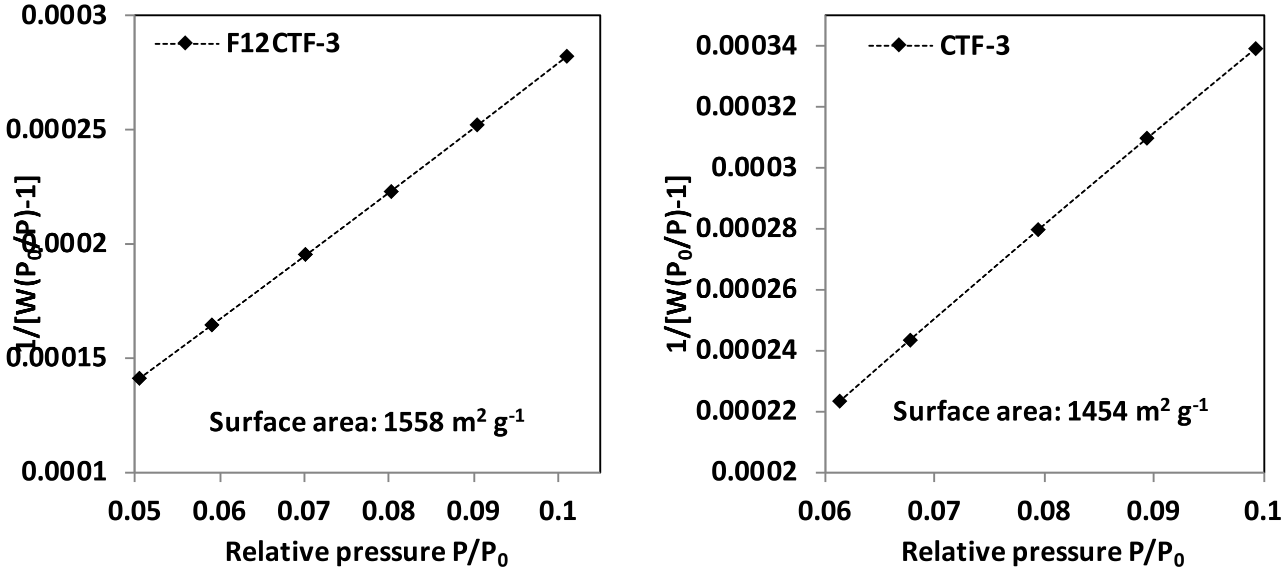

**Figure S6** BET plots of **$F_{12}$CTF-3** and **CTF-3**.

**Table S1** Summarization of various solid physisorbents with $CO_2$ capacities > 5.0 mmol $g^{-1}$ at 273 K and 1 bar.

| Sample | $S_{BET}$($m^2$ $g^{-1}$) | $CO_2$ uptake (mmol $g^{-1}$) | | Reference |
|---|---|---|---|---|
| | | 273 K | 298 K | |
| $F_{12}$CTF-3 | 1759 | 6.58 | 4.33 | This work |
| PPF-1 | 1740 | 6.07 | 3.35 (295 K) | [7] |
| Bipy-CTF600 | 2479 | 5.58 | 2.95 | [8] |
| HAT-CTF-450/600 | 1090 | 6.3 | 4.8 (297 K) | [6] |
| SU-MAC-500 | 941 | 6.03 | 4.50 | [9] |
| F-DCBP-CTF-1 | 2437 | 5.98 | 3.82 | [10] |
| FCTF-1-600 | 1535 | 5.53 | 3.41 | [11] |
| F-MOP-2 | 1031 | 5.07 | 1.55 | [12] |
| BILP-3 | 1306 | 5.11 | 3.30 | [13] |
| BILP-4 | 1135 | 5.34 | 3.59 | [14] |
| BILP-12 | 1497 | 5.07 | 3.18 | [15] |
| TBILP-2 | 1080 | 5.18 | 3.32 | [16] |
| TB-COP-1 | 1340 | 5.19 | 3.16 | [17] |
| ALP-1 | 1235 | 5.36 | 3.25 | [18] |
| NPOF-1-$NH_2$ | 1535 | 5.84 | 3.77 | [19] |
| Fe-POP-2 | 855 | 5.10 | - | [20] |
| CQN-1g | 1870 | 7.16 | 4.57 | [21] |

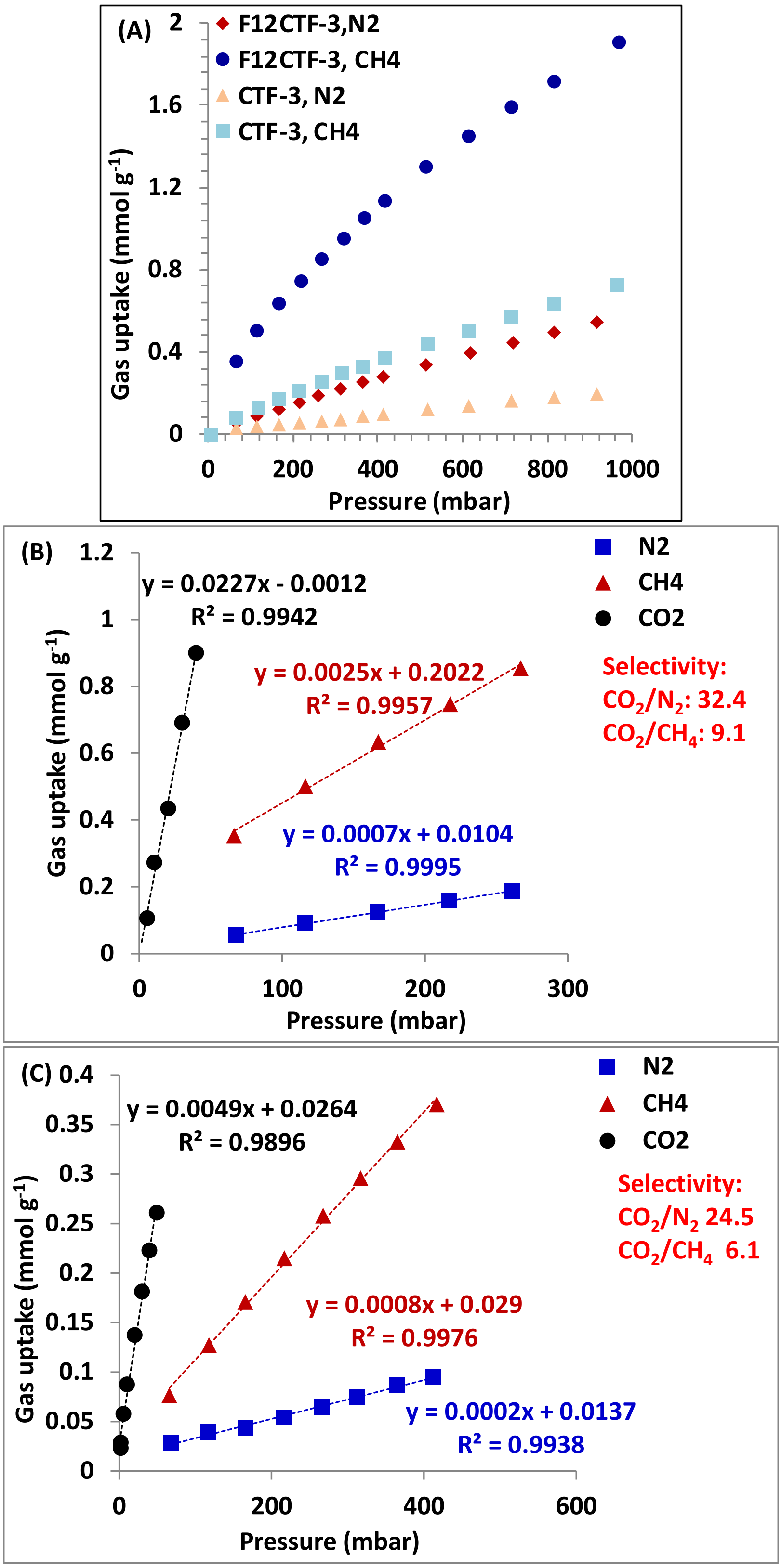

**Figure S7** (A) $N_2$ and $CH_4$ uptake by **$F_{12}$CTF-3** and **CTF-3** at 273 K. (B) $CO_2/N_2$ and $CO_2/CH_4$ selectivities at 273 K by **$F_{12}$CTF-3** and (C) **CTF-3** calculated by the ratio of the initial slopes of the $CO_2$, $N_2$ and $CH_4$ adsorption isotherms.

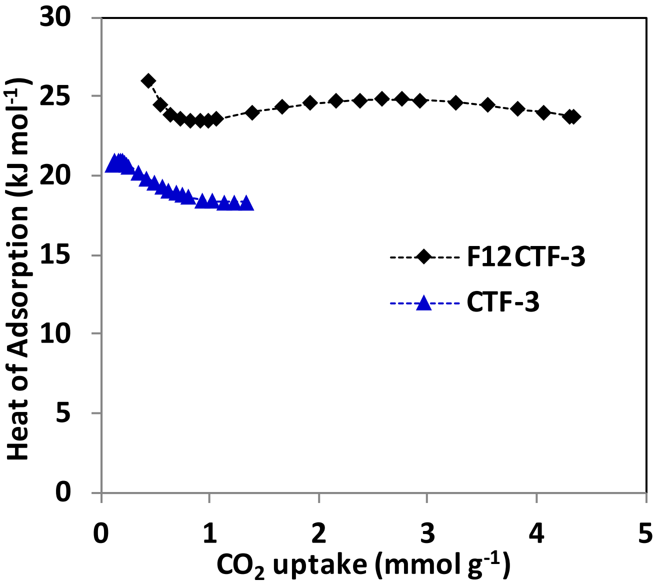

**Figure S8** Isosteric heats of adsorption ($Q_{st}$) for $CO_2$ adsorption by **$F_{12}$CTF-3** and **CTF-3.** The isosteric heats of adsorption ($Q_{st}$) are calculated by fitting the $CO_2$ adsorption isotherms at 273 K and 298 K and applying of the Clausius-Clapeyron equation.

**Table S2** CO$_2$ uptake capacities of **F$_{12}$CTF-3** prepared at different reaction temperatures

| Sample | S$_{BET}$ (m$^2$ g$^{-1}$) | Vtotal (cm$^3$ g$^{-1}$) | CO$_2$ uptake (mmol g$^{-1}$) |  |  |  | Q$_{st}$ (kJ mol$^{-1}$)[a] | F Content (wt%)[b] | N Content (wt%)[b] |
|---|---|---|---|---|---|---|---|---|---|
|  |  |  | 273 K |  | 298 K |  |  |  |  |
|  |  |  | 0.15 bar | 1 bar | 0.15 bar | 1 bar |  |  |  |
| **F$_{12}$CTF-3-350** | 842 | 0.72 | 0.62 | 1.79 | 0.34 | 1.16 | 26.4 | 16.06 | 7.91 |
| **F$_{12}$CTF-3-450** | 1881 | 1.35 | 1.91 | 6.43 | 1.04 | 3.99 | 24.2 | 7.00 | 6.37 |
| **F$_{12}$CTF-3-450/600** | 1558 | 1.32 | 2.45 | 6.58 | 1.38 | 4.33 | 24.5 | 3.70 | 5.5 |
| **F$_{12}$CTF-3-600** | 1656 | - | 2.40 | 6.47 | 1.30 | 4.07 | 26.8 | - |  |
| **F$_{12}$CTF-3-450/800** | 2085 | 1.77 | 1.26 | 4.70 | 0.78 | 3.18 | 18 | 2.74 | 3.22 |

[a] Data corresponding to CO$_2$ capacity of 0.5 mmol g$^{-1}$. [b] Obtained by XPS measurement. The content of F and N in the monomer F$_{12}$CN-3 was 38.2 wt% and 7.0 wt%, respectively.

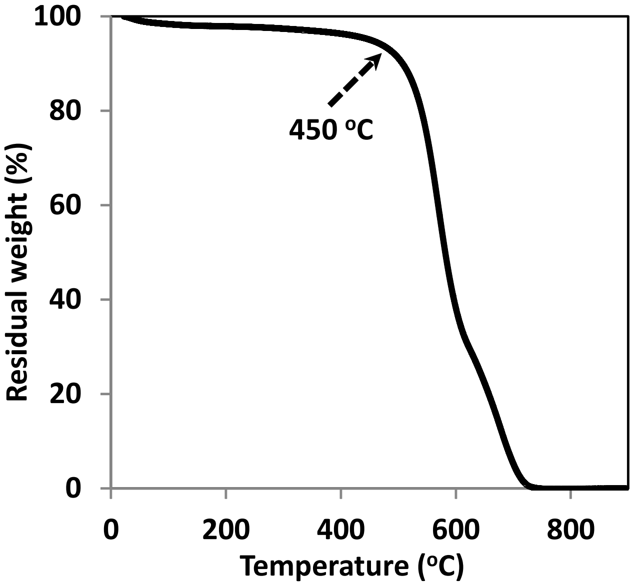

**Figure S9** Thermogravimetric analysis (TGA) result of **$F_{12}$CTF-3-350** under air up to 900 °C at a ramping rate of 10 °C min$^{-1}$.

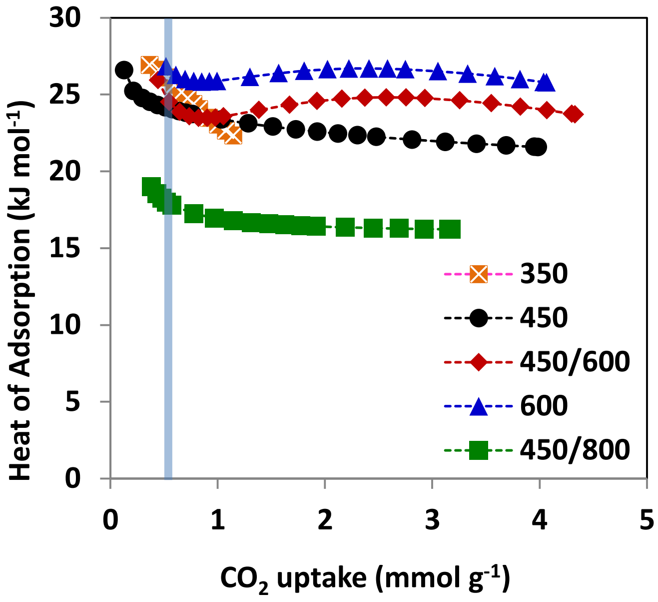

**Figure S10** Isosteric heats of adsorption (Qst) for $CO_2$ adsorption by **$F_{12}$CTF-3** obtained at different reaction temperatures.

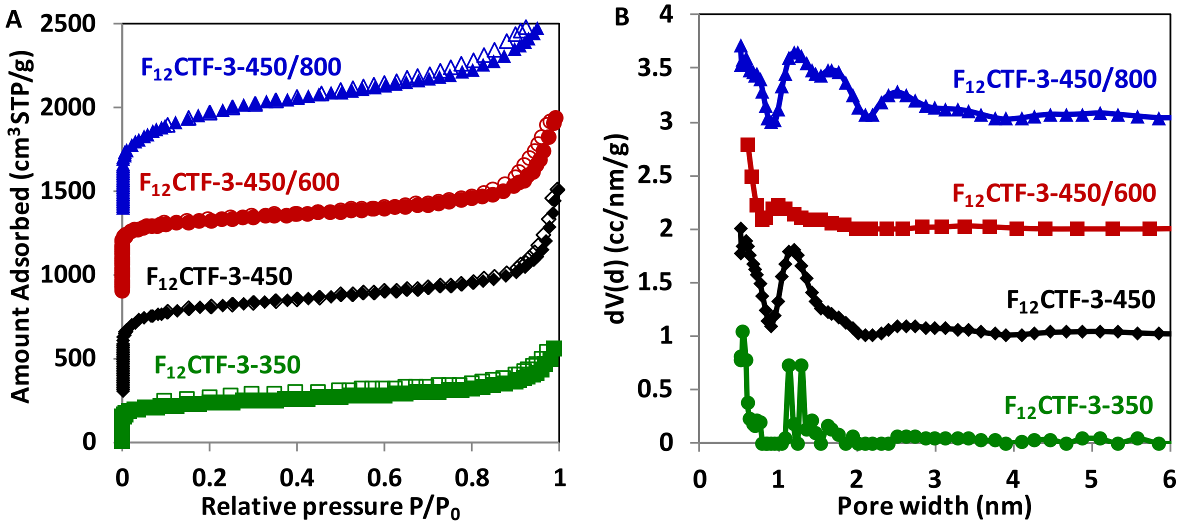

**Figure S11** (A) $N_2$ isotherms at 77 K and (B) pore size distributions of **$F_{12}$CTF-3** obtained at different ionothermal reaction temperatures.

**Table S3** $CO_2$ uptake capacities of **O-CTF-3** and **O-CTF-2** with different F content within the backbone.

| Sample | $S_{BET}$($m^2$ $g^{-1}$) | $CO_2$ uptake (mmol $g^{-1}$)<br>273 K | | 298 K | |
|---|---|---|---|---|---|
| | | 0.15 bar | 1 bar | 0.15 bar | 1 bar |
| O-CTF-3 | 1450 | 1.06 | 3.17 | 0.53 | 1.70 |
| O-$F_3$CTF-3 | 1886 | 1.08 | 3.61 | 0.60 | 2.21 |
| O-$F_6$CTF-3 | 1874 | 1.36 | 4.45 | 0.75 | 2.86 |
| O-$F_{12}$CTF-3 | 1822 | 1.77 | 5.59 | 0.81 | 3.04 |
| O-CTF-2 | 1130 | 0.83 | 2.65 | 0.63 | 2.06 |
| O-$F_8$CTF-2 | 1878 | 0.96 | 3.47 | 0.62 | 2.31 |
| O-$F_8$CTF-2’ | 1403 | 1.04 | 3.61 | 0.61 | 2.30 |
| O-$F_{16}$CTF-2 | 948 | 1.86 | 5.10 | 1.03 | 3.30 |

**Table S4** Elemental analysis (C, H, N and F) of **O-CTF-2** with different F content within the backbone.

| Sample | $S_{BET}$ (m$^2$ g$^{-1}$) | Elemental content in materials | | | | Elemental content in monomers | | | |
|---|---|---|---|---|---|---|---|---|---|
| | | C | H | N | F | C | H | N | F |
| **O-CTF-2** | 1130 | 81.34 | 1.92 | 2.69 | - | 80.4 | 4.1 | 7.2 | - |
| **O-F$_8$CTF-2** | 1878 | 69.26 | 2.97 | 4.08 | 0.78 | 58.7 | 1.5 | 5.3 | 28.6 |
| **O-F$_8$CTF-2'** | 1403 | 71.40 | 2.51 | 4.24 | 4.46 | 58.7 | 1.5 | 5.3 | 28.6 |
| **O-F$_{16}$CTF-2** | 948 | 53.02 | - | 5.40 | 16.84 | 46.2 | - | 4.1 | 44.9 |

**$F_{12}$CTF-3, 0.62 nm**

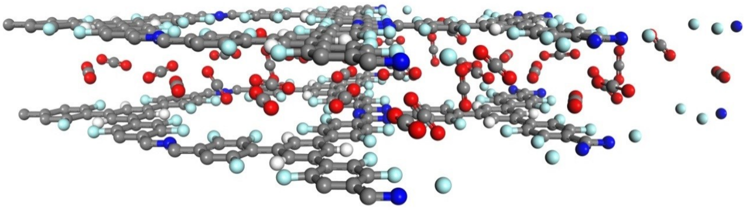

**$F_{12}$CTF-3, 0.71 nm**

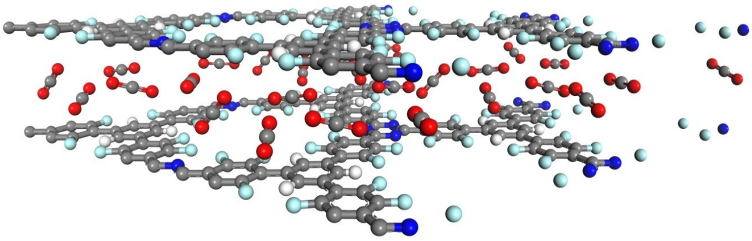

**CTF-3, 1.0 nm**

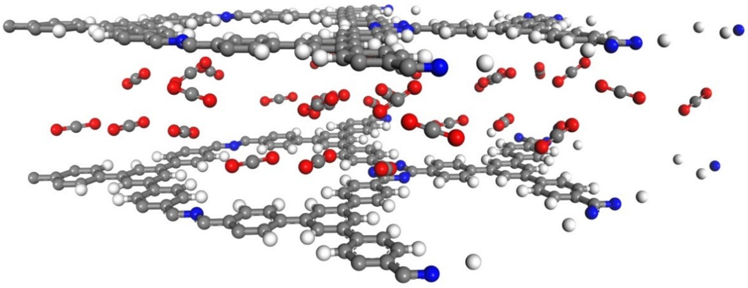

## CTF-3, 3.0 nm

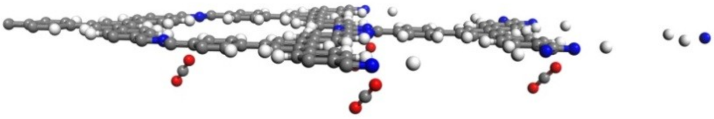

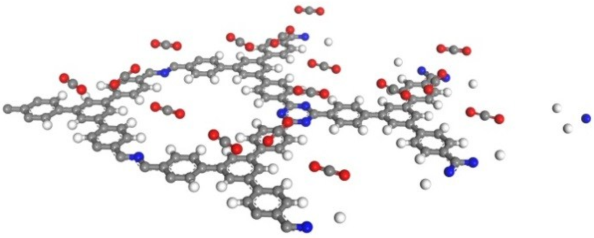

**Figure S12** The snapshots of $CO_2$ distribution at 1 bar using **$F_{12}$CTF-3** and **CTF-3**.

**Table S5** Element contents (C, N, H, F) and molecular weights of CTF materials used for $CO_2$ uptake prediction.

| Sample | Element content (wt%) | | | | $CO_2$ capacity (mmol $g^{-1}$) | |
|---|---|---|---|---|---|---|
| | C | N | H | F | 273 K | 298 K |
| **CTF-3** | 85.0 | 11.0 | 3.9 | 0 | 10.60 | 6.47 |
| **$F_1$CTF-3** | 81.2 | 10.5 | 3.5 | 4.76 | 10.88 | 6.86 |
| **$F_3$CTF-3** | 74.5 | 9.7 | 2.8 | 13.1 | 9.22 | 5.75 |
| **$F_6$CTF-3** | 66.3 | 8.6 | 1.8 | 23.3 | 7.57 | 4.71 |
| **$F_{12}$CTF-3** | 54.3 | 7.0 | 0.5 | 38.2 | 6.70 | 4.13 |

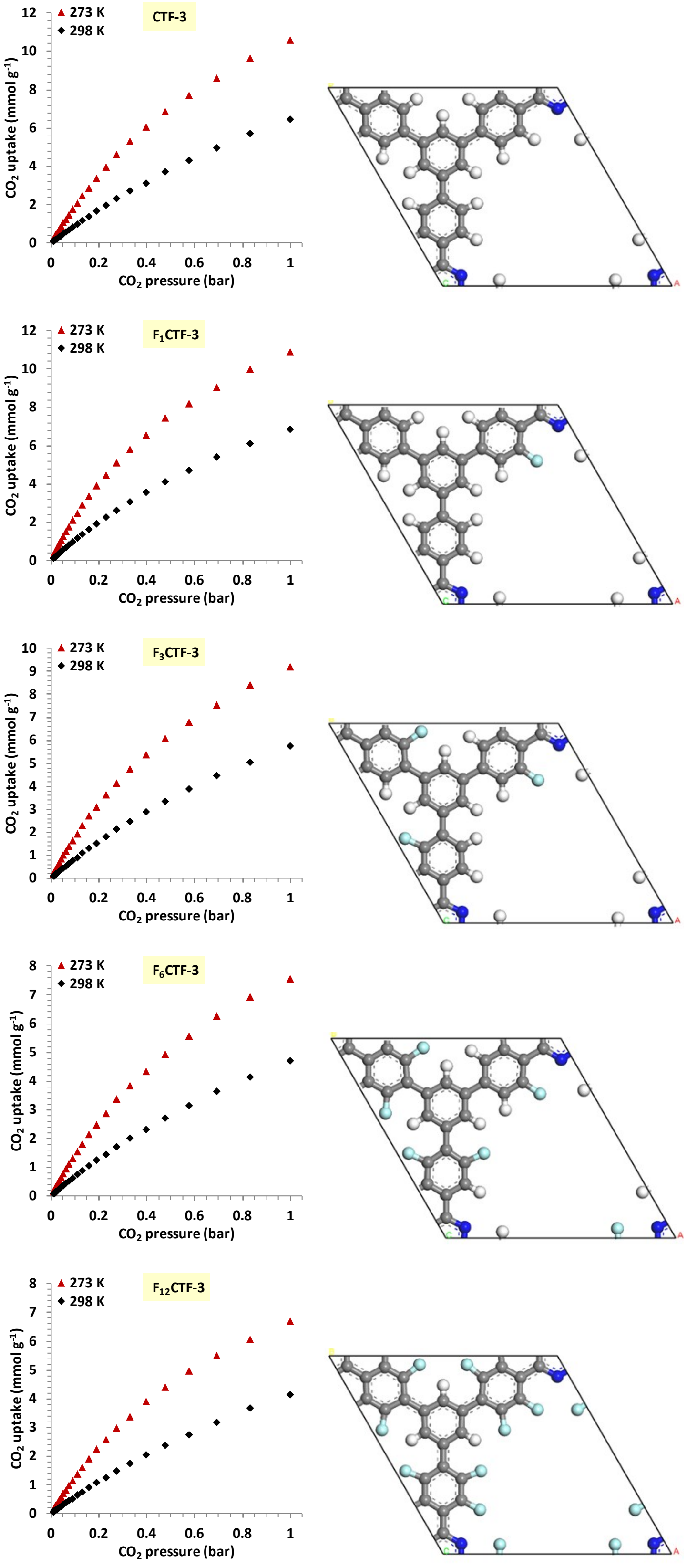

**Figure S13** Structural models of CTF materials used for CO$_2$ uptake prediction and the obtained CO$_2$ adsorption curves.

**Table S6** Comparison of the experimental results and $CO_2$ uptake capacities predicted using a deep learning method.

| Sample | $S_{BET}$ | $V_{total}$ | $V_{micro}$ | Predicted $CO_2$ uptake[a] | | Experimental results | |
|---|---|---|---|---|---|---|---|
| | | | | 273 K | 298 K | 273 K | 298 K |
| **CTF-3** | 1454 | 1.32 | 0 | 0.55 | 0.77 | 2.13 | 1.34 |
| **$F_{12}$CTF-3** | 1558 | 0.98 | 0.43 | 5.07 | 3.14 | 6.58 | 4.33 |
| **$F_{12}$CTF-3-350** | 842 | 0.72 | 0.20 | 3.41 | 2.15 | 1.79 | 1.16 |
| **$F_{12}$CTF-3-450** | 1881 | 1.35 | 0.47 | 5.02 | 2.98 | 6.43 | 3.99 |
| **$F_{12}$CTF-3-450/800** | 2085 | 1.77 | 0.17 | 2.28 | 2.06 | 4.70 | 3.18 |

[a] The predicted $CO_2$ uptake is determined via deep neural network trained from over 1000 data set.

The deep learning neural network (DNN) with two hidden layers was created in MATLAB R2018a environment using backpropagation algorithm according to our previous study.[22] The weights and biases were the key two paremeters to determine neural network sturcture. The neural network was allowed to adjust the weight and biases value during training process to improve their performance. Neurons arranged in layers were needed to be connected each other into a neural network. Each neuron is usually a simple processing unit with many inputs to produce an output. The selection of neurons was significantly important. In our study, a part of $S_{BET}$, $V_{micro}$ and $V_{meso}$ as well as the adsorption conditions (temperature and pressure) were selected as the input neurons. And $CO_2$ adsorption capacity was chosen as the output neuron. Before the creation, the inputs and outputs are normalized in the range of 0 to 1. For simplicity, we assume that two hidden layers for DNN was chosen in our work, and the hidden neuron numbers were optimized by comparing the results derived from different hidden neurons numbers. Backpropagation training method was used to train the neural networks. Training numbers was chosen less than 100000, and goal errors was chosen as 0.001 according to the reported study. And then, the predicted data was achieved using linear or nonlinear combination of the input vector, weights, biases and transfer functions. Among these analysisthe selected neuron number of hidden layers was 8 and 8 respectively according to the optimized results.

## 3 Reference

[1] D. D. Dixon, D. Sethumadhavan, T. Benneche, A. R. Banaag, M. A. Tius, G. A. Thakur, A. Bowman, J. T. Wood, A. Makriyannis, *J. Med. Chem.* **2010**, *53*, 5656-5666.

[2] P. Li, Y. He, Y. Zhao, L. Weng, H. Wang, R. Krishna, H. Wu, W. Zhou, M. O'Keeffe, Y. Han, B. Chen, *Angew. Chem. Int. Ed.* **2015**, *54*, 574-577.

[3] M. I. Hashim, H. T. M. Le, T.-H. Chen, Y.-S. Chen, O. Daugulis, C.-W. Hsu, A. J. Jacobson, W. Kaveevivitchai, X. Liang, T. Makarenko, O. Š. Miljanić, I. Popovs, H. V. Tran, X. Wang, C.-H. Wu, J. I. Wu, *J. Am. Chem. Soc.* **2018**, *140*, 6014-6026.

[4] T.-H. Chen, I. Popov, O. Zenasni, O. Daugulis, O. S. Miljanic, *Chem. Commun.* **2013**, *49*, 6846-6848.

[5] S. Roy, K. Biradha, *Aust. J. Chem.* **2013**, *66*, 436-442.

[6] X. Zhu, C. Tian, G. M. Veith, C. W. Abney, J. Dehaudt, S. Dai, *J. Am. Chem. Soc.* **2016**, *138*, 11497-11500.

[7] Y. Zhu, H. Long, W. Zhang, *Chem. Mater.* **2013**, *25*, 1630-1635.

[8] S. Hug, L. Stegbauer, H. Oh, M. Hirscher, B. V. Lotsch, *Chem. Mater.* **2015**, *27*, 8001-8010.

[9] J. W. F. To, J. He, J. Mei, R. Haghpanah, Z. Chen, T. Kurosawa, S. Chen, W.-G. Bae, L. Pan, J. B. H. Tok, J. Wilcox, Z. Bao, *J. Am. Chem. Soc.* **2016**, *138*, 1001-1009.

[10] G. Wang, K. Leus, H. S. Jena, C. Krishnaraj, S. Zhao, H. Depauw, N. Tahir, Y.-Y. Liu, P. Van Der Voort, *J. Mater. Chem. A* **2018**, *6*, 6370-6375.

[11] Y. Zhao, K. X. Yao, B. Teng, T. Zhang, Y. Han, *Energy Environ. Sci.* **2013**, *6*, 3684-3692.

[12] Z.-Z. Yang, Y. Zhao, H. Zhang, B. Yu, Z. Ma, G. Ji, Z. Liu, *Chem. Commun.* **2014**, *50*, 13910-13913.

[13] M. G. Rabbani, T. E. Reich, R. M. Kassab, K. T. Jackson, H. M. El-Kaderi, *Chem. Commun.* **2012**, *48*, 1141-1143.

[14] M. G. Rabbani, H. M. El-Kaderi, *Chem. Mater.* **2012**, *24*, 1511-1517.

[15] A. K. Sekizkardes, T. İslamoğlu, Z. Kahveci, H. M. El-Kaderi, *J. Mater. Chem. A* **2014**, *2*, 12492-12500.

[16] A. K. Sekizkardes, S. Altarawneh, Z. Kahveci, T. İslamoğlu, H. M. El-Kaderi, *Macromolecules* **2014**, *47*, 8328-8334.

[17] J. Byun, S.-H. Je, H. A. Patel, A. Coskun, C. T. Yavuz, *J. Mater. Chem. A* **2014**, *2*, 12507-12512.

[18] P. Arab, M. G. Rabbani, A. K. Sekizkardes, T. İslamoğlu, H. M. El-Kaderi, *Chem. Mater.* **2014**, *26*, 1385-1392.

[19] T. Islamoglu, T. Kim, Z. Kahveci, O. M. El-Kadri, H. M. El-Kaderi, *J. Phys. Chem. C* **2016**, *120*, 2592-2599.

[20] A. Modak, M. Nandi, J. Mondal, A. Bhaumik, *Chem. Commun.* **2012**, *48*, 248-250.

[21] O. Buyukcakir, R. Yuksel, Y. Jiang, S. H. Lee, W. K. Seong, X. Chen, R. S. Ruoff, *Angew. Chem. Int. Ed.* **2018**, DOI: 10.1002/anie.201813075.

[22] Z. Zhang, J. A. Schott, M. Liu, H. Chen, X. Lu, B. G. Sumpter, J. Fu, S. Dai, *Angew. Chem. Int. Ed.* **2019**, *58*, 259-263.